




Microstructural characterization and mechanical properties of a Q550W weathering steel welded joint under different heat inputs

Tianen Peng¹, Chao Fu¹, Zhuobin Qin¹, Bo He², Xuewen Hu², Tao Zhu², Bo Jiang^{1,*} , and Yazheng Liu¹

¹School of Materials Science and Engineering, University of Science and Technology Beijing, Beijing 100083, China

²Technical Center, Maanshan Iron & Steel Co. Ltd, Maanshan 243041, China

Received: 14 June 2022

Accepted: 24 August 2022

Published online:

2 September 2022

© The Author(s), under exclusive licence to Springer Science+Business Media, LLC, part of Springer Nature 2022

ABSTRACT

Metal active gas arc (MAG) was applied to weld a hot-rolled weathering steel, three heat inputs (5100, 6000 and 7200 J/cm) were used by changing the welding speed. The effects of heat input on the microstructure on the welded joint were investigated by optical microscope (OM), field emission scanning electron microscope (FESEM), electron-backscattering diffraction (EBSD). Tensile and hardness tests were also carried out in this paper. The results indicate that the yield strength decreases with the increase in heat input and all the specimen fractured at the mixed-grained heat affected zone (MGHAZ). The MGHAZ consist of polygonal and equiaxed ferrite. The yield strength decreases by 59 MPa when the heat input increases from 5100 to 7200 J/cm, which is attributed to the weakening of grain refinement strengthening and dislocation strengthening. The plasticity also decreases by 3.6% with the increase in heat input. The microstructure is relatively uniform when the heat input is 5100 J/cm. However, the original microstructure become coarsen with the increase in heat input, resulting the non-uniform microstructure at higher heat input. The 5100 J/cm specimen could deform more coordinately during tensile process, so the specimen has highest plasticity among three heat inputs.

Introduction

The corrosion resistance of weathering steel has been enhanced by the addition of P, Ni, Cr and Cu. It has been widely applied for structural steel, such as

vehicles, bridges, towers and equipment exposed to the atmosphere for a long time [1, 2]. The 550 MPa grade weathering steel has been widely used in structural steel due to its combination of high strength and low production costs [3, 4]. In the

Handling Editor: Catalin Croitoru.

Address correspondence to E-mail: jiangbo@ustb.edu.cn

practical application, most of the weathering steel has been welded to manufacture typical components. However, the welding thermal cycle is characterized by rapid heating, uneven cooling rate with a high peak temperature, which may coarsen the microstructure and deteriorate the balance of strength and plasticity [5, 6]. Therefore, it is worthy to explore proper parameters for the welding of high strength weathering steel.

Generally speaking, the factors influencing the quality of the welding of the structural steel mainly include welding methods [7–9], welding parameters [10–13], welding materials [14], chemical composition of base metal [15–17]. Welding parameters play an essential role in determining the mechanical properties and microstructure of structural steel after welding. Zhao et al. [10] investigated the influence of heat input on the mechanical properties of A606 weathering steel by gas metal arc welded (GMAW). The result showed that the microstructure in fusion zone (FZ) and heat affected zone (CGHAZ) coarsened with the increase in heat input, so the hardness of the CGHAZ and FZ declined owing to the growth of the coarsened grains. Wang et al. [11] studied a hot-rolled Nb-Ti-Mo microalloyed steel by hybrid fiber laser arc welding and three heat inputs (3.90, 5.20 and 7.75 kJ/cm) were used in this study. They found that the microstructure in FZ mainly consisted of lath martensite when the heat input was 3.90 and 5.20 kJ/cm. However, the content of martensite decreased and that of the granular bainite (GB) increased when the heat input was 7.75 kJ/cm. The different microstructures caused the non-uniform strain distribution during the tensile process, thus to cause the decrease in strength and plasticity. Wen et al. [12] investigated the microstructure and mechanical properties of structural steel with different heat inputs, and the heat inputs were 7.5, 10.5, 14.5 and 18.5 kJ/cm, respectively. The results showed that the microstructure of weld metal (WM) consisted of high volume fraction of acicular ferrite regardless of heat input. However, the acicular ferrite changed from bainite acicular ferrite (B-AF) to Widmanstätten acicular ferrite (WF-AF) with the increase in heat input. This change would cause the decrease in dislocation density and the increase in effective grain size, thus to cause the decrease in strength. Wang et al. [13] studied the effect of welding heat input (10, 25, 40 and 55 kJ/cm) on microstructure and impact toughness in CGHAZ of X100Q steel. They found that the

prior austenite grain and the bainitic lath was refined with the decrease in heat input. Therefore, the impact toughness was enhanced due to the refined microstructure. From the above analysis, we can conclude that the optimum welding parameters are different for steels with different compositions and strength. In addition, there is no detailed study on the relationship between strength and microstructure of 550 MPa high strength weathering steel. Therefore, it is essential to carry out a study on the parameters-property relationship of high strength weathering steel.

In this paper, a 550 MPa grade weathering steel treated by metal active gas arc (MAG) welding was investigated. The aim of this study is to elucidate microstructural evolution of welded joints with different heat inputs in detail and establish a relationship between microstructure and mechanical properties of welded joints.

Experimental

Materials

Table 1 shows the chemical composition of the base metal and welding wire. The carbon content of base metal is extremely low in order to obtain excellent solderability [18, 19] and the Ti microalloying method is adopted to achieve the high strength [20]. The composition of welding wire is close to the base metal, but the Mn and Ni is slightly higher to ensure strength, plasticity and corrosion resistance after welding [21–23]. The base metal was produced by rolling and coiling process, the final thickness is 4 mm. The heating temperature, final rolling temperature and coiling temperature are 1250, 890 and 620 °C, respectively. The yield strength of base metal and welding wire are 574 MPa and 580 MPa, respectively. The equivalent carbon content (C_{eq}) and the welding crack susceptibility index (P_{cm}) of base metal were calculated using Eqs. (1) and (2) [24, 25]. The value of C_{eq} and P_{cm} are 0.268% and 0.209%, respectively. The weldability and crack susceptibility of welded joints are determined by C_{eq} and P_{cm} [26]. The solderability is excellent if the value of C_{eq} and P_{cm} are lower than 0.4% and 0.25%. Therefore, pre-heating process is not necessary before welding.

Table 1 Chemical compositions of the base metal and welding wire (mass fraction, %)

	C	Si	Mn	P	S	Als	Cu	Cr	Ni	Ti
Base metal	0.069	0.47	0.50	0.023	0.006	0.019	0.25	0.45	0.14	0.060
Welding wire	≤ 0.11	0.40–0.80	1.60–1.90	≤ 0.25	≤ 0.25	–	≤ 0.50	0.20–0.60	2.00–2.50	≤ 0.12

$$C_{eq} = C + \frac{Mn}{6} + \frac{Ni + Cu}{15} + \frac{Cr + Mo + V}{5} \quad (1)$$

$$P_{cm} = C + \frac{Si}{6} + \frac{Mn + Cu + Cr}{20} + \frac{Ni}{60} + \frac{Mo}{15} + \frac{V}{10} + 5B \quad (2)$$

Welding methods

The semi-automatic arc welding machine was employed to carry out welding process with shielding gas consisting of CO₂. According to previous studies in the laboratory, the welding current and voltage were set as 200 A and 18 V, respectively. This parameter can ensure fine microstructures and excellent mechanical properties after welding. Welding speed is an important parameter in welding process, a proper speed could produce a great extent of constitutional supercooling at the solidification front and this in turn helps heterogeneous nucleation, which is responsible for grain refining in the welded joint. In this paper welding speed is regarded as a variable, the speeds are set as 0.5, 0.6 and 0.7 cm/s, respectively. The heating inputs can be calculated using Eq. (3) [27]:

$$E = \frac{UI}{v} \quad (3)$$

where E is heat input (J·cm⁻¹), U and I are voltage (V) and current (A), respectively. v is welding speed (cm s⁻¹). From Eq. (3), the calculated heat inputs are 5100, 6000 and 7200 J·cm⁻¹, respectively. The detailed parameters are listed in Table 2. The plate was cut into several pieces with the dimensions of 450 mm (length) × 60 mm (width) × 4 mm (thickness), a single V-type butt groove was machined in these

pieces. The welding direction was perpendicular to the rolling direction of the sample, as shown in Fig. 1a. The specimens for tensile testing, hardness testing and microstructural observation were taken from the welded plate, as schematically illustrated in Fig. 1b.

Microstructural observation and mechanical properties testing

The samples were grounded, polished and etched with 4% nital for 10 s as per GB/T 26,955–2011. The microstructure was observed by optical microscope (OM, model: Zeiss Scope A1), field emission scanning electron microscopy (SEM, Gemini 500). Microhardness tester (VTD512) was used to test the hardness of each zone in the weld joints, the loading was 200 g and 15 s for holding time. The test location was 1 mm from the top surface of the welded joint. Hardness testing was conducted with an interval of 0.2 mm between test points.

Each tensile specimen size was prepared in accordance with GB/T 2651–2008 standard and welded seam was located in the center, as shown in Fig. 1b. Tensile tests were carried out using WDW200D universal material testing machine at a crosshead speed of 3 mm/min. In order to analyze the fracture behavior, the tensile specimens with 5100 and 7200 J/cm were observed by SEM. In addition, the SEM was also used for secondary electron imaging and electron backscatter diffraction (EBSD) measurements of the specimen. The observations were carried out from two directions: (1) toward the specimen surface and (2) toward a longitudinal section (Fig. 1c).

Table 2 Detailed parameters for each specimen

No	Welding current/A	Welding voltage/V	Welding speed/cm s ⁻¹	Heat input/J cm ⁻¹
1	200	18	0.7	5100
2	200	18	0.6	6000
3	200	18	0.5	7200

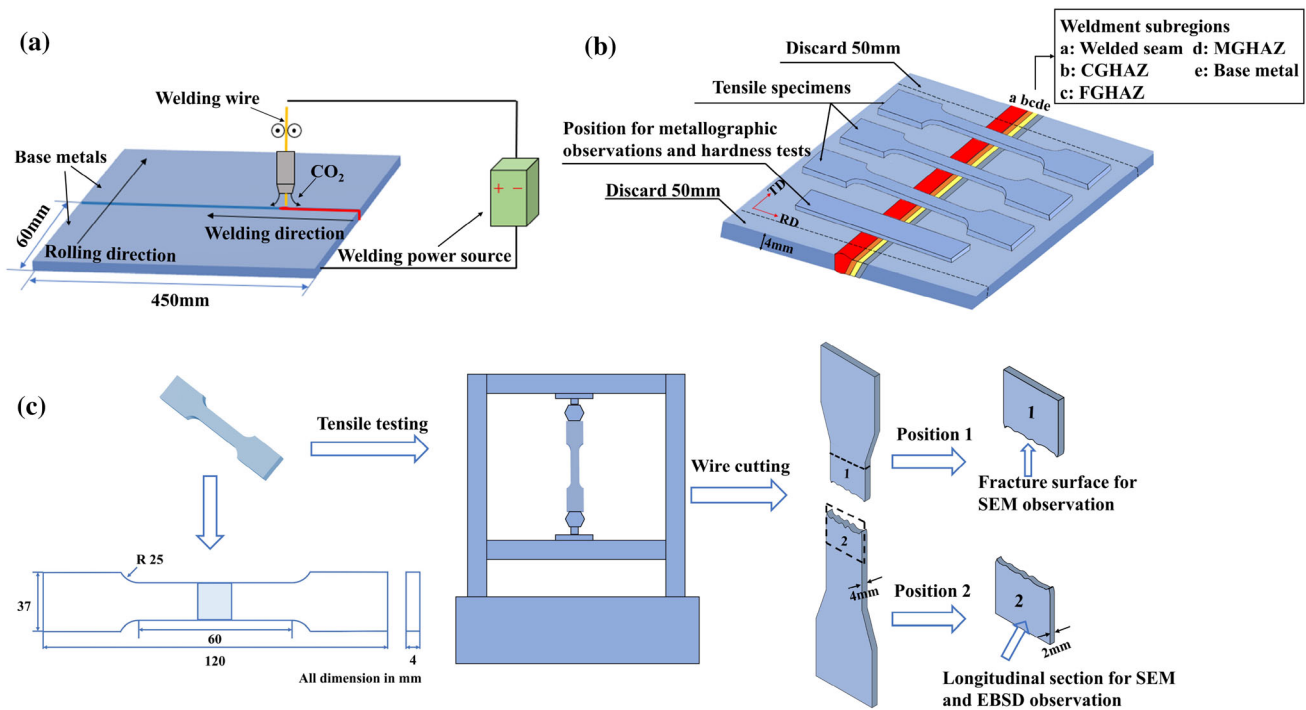


Figure 1 Schematic diagram of experimental process. **a** Schematic of welding process; **b** Schematic of the location for tensile, hardness and metallographic specimens; **c** Schematic of the observed section of tensile specimens.

Results and discussion

Effect of heat inputs on the microstructure of welded joints

Effect of heat inputs on the microstructure of welded seam, CGHAZ and FGHAZ

Figure 2a shows the schematic diagram of the microstructure in welded joints, the temperature varies with the distance from the welded seam. The microstructure of the welded joints can be divided into three zones: welded seam, heat affected zone (HAZ) and base metal. According to the distance to the welded seam, HAZ can be categorized into a coarse-grained HAZ (CGHAZ), fine-grained HAZ (FGHAZ) and mixed-grained HAZ (MGHAZ). The microstructure of base metal is also shown in Fig. 2a, it is mainly composed of elongated polygonal ferrite (PF). Besides, there also exist a small fraction of degenerate pearlite (DP). The average grain size of the ferrite is 10.4 μm.

Various phase transformation would be occurred after welding due to the different heating temperature. The microstructure of the welded seam under different heat inputs is shown in Fig. 2b–d. The

microstructure consists of lath bainite (LB) and granular bainite (GB). The lath of bainite become thick with the increase in heat inputs, besides, the content of granular bainite is also increased. The width of bainite lath was measured using SEM micrographs taken from 10 different locations in welded seam for each heat input condition, the average bainite width is shown in Fig. 2l. The increase in heat input would result in the decrease in cooling rate [28]. Low heat input means that the faster cooling rate after welding, thus to cause the decrease in transformation temperature. Hence, the subcooling degree is increased and the energy required for nucleation is decreased. This means the lower heat input would refine the bainite lath [29]. Due to the higher transformation temperature of granular bainite, the rise of heat input would increase the transformation temperature, which would promote the formation of granular bainite at higher heat input [30].

The coarse-grained HAZ is next to the welded seam. The heating temperature range in this region is about 1000 to 1400 °C. The temperature is so high that the austenite grain grows seriously, thus the coarsened grains are obtained after cooling. According to Fig. 2e–g, the microstructure is nearly all granular

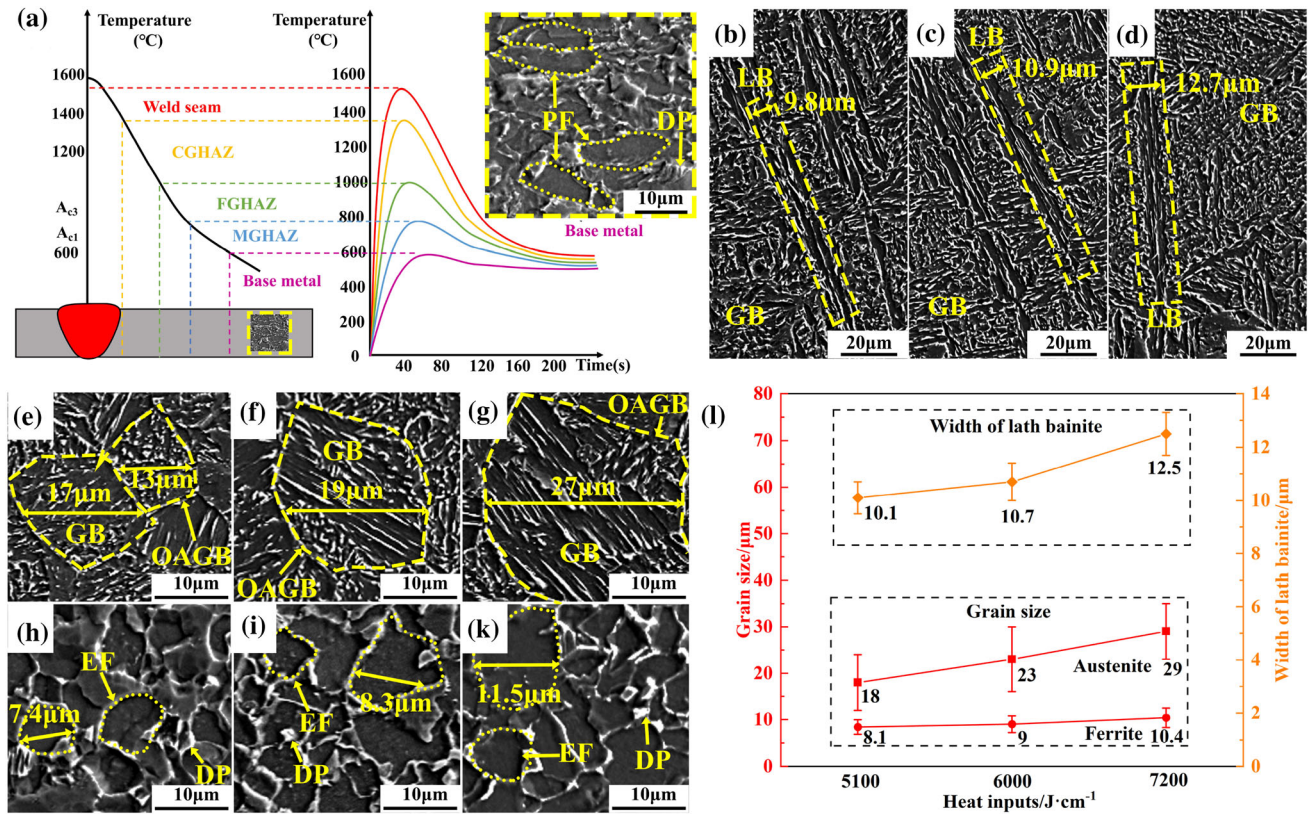


Figure 2 Microstructure of welded joints under different heat inputs. **a** Schematic diagram of the microstructure in welded joints; **b–d** microstructure of welded seam; **e–g** microstructure of

CGHAZ; **h–k** microstructure of FGHAZ; **l** measured value of grain size and width of bainite lath.

bainite under three heat inputs. Moreover, the size of original austenite grain boundary (OAGB) increases with the increase in heat input. The original austenite grain size under the heat inputs of 5100, 6000 and 7200 J/cm is 18, 23 and 29 μm , respectively (Fig. 2l). The higher heat input would coarsen the austenite grain size. Besides, the increase in heat input decreases the cooling rate, so the residence time of austenite at high temperature was prolonged and the grain was coarsened [31].

The area next to the coarse-grained HAZ is fine-grained HAZ. The heating temperature in this region is between A_{c3} and 1000 $^{\circ}C$. During welding process, the microstructure of base metal all transformed into austenite, and the dislocation density is decreased. As the heating temperature is slightly higher than A_{c3} , the austenite grain size is relatively small, thus uniform and fine ferrite is obtained after cooling. The microstructure of fine-grained HAZ consists of equiaxed ferrite (EF) and small percentage of degenerate pearlite under all heat inputs (Fig. 2h–k). The average grain size is 8.1, 9 and 10.4 μm (Fig. 2l).

It can be seen that the grain size is slightly coarser as the heat input increased.

Effect of heat inputs on the microstructure of MGHAZ

The microstructure of the mixed-grained HAZ is shown in Fig. 3. The microstructure of mixed-grained HAZ is mainly composed of equiaxed ferrite and polygonal ferrite. The equiaxed ferrite is similar to the microstructure in fine-grained HAZ and polygonal ferrite is similar to microstructure in base metal. It can also be seen that the grain non-uniformity increases gradually with the increase in heat input (Fig. 3c, f, i). The ferrite grain size is in the range of 3 to 16 μm and the average diameter is 8.6 μm when the heat input is 5100 J/cm . However, the size distribution is in the range of 3 to 22 μm and the average diameter is 11.3 μm when the heat input increased to 7200 J/cm . The variance of grain size under three heat inputs are 2.5, 3.1 and 4.3 μm^2 , respectively. It shows that the grain size is more non-uniform at higher heat input.

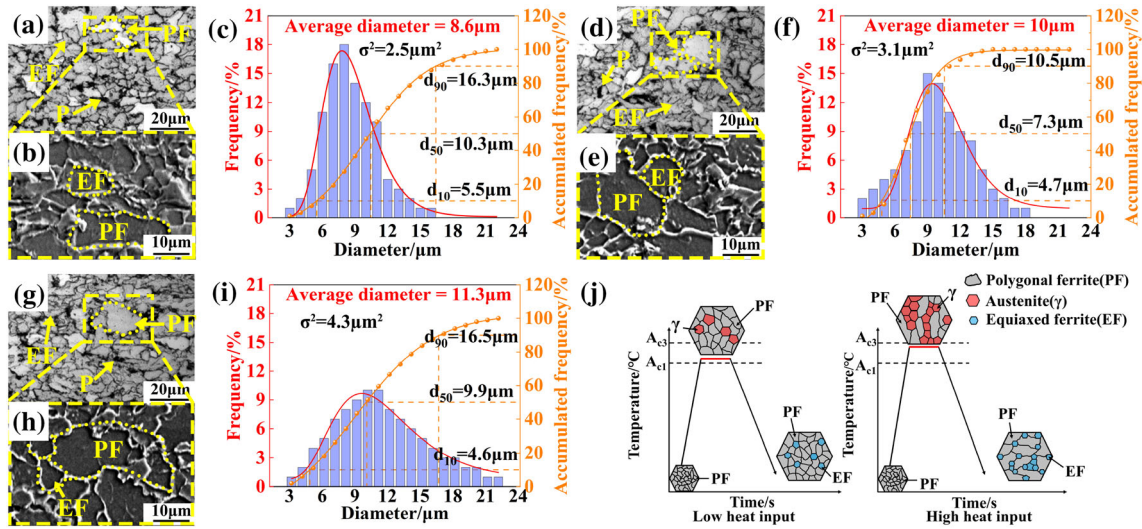


Figure 3 Microstructure of MGHAZ under different heat inputs. **a–c** 5100 J/cm; **d–f** 6000 J/cm; **g–i** 7200 J/cm; **j** schematic diagram of the phase transformation in MGHAZ.

The reason for the difference of microstructure under three heat inputs can be explained in Fig. 3j. The heating temperature in this region is between A_{c1} and A_{c3} . Only a part of the microstructure in this region transformed to austenite, fine and equiaxed grains were obtained after cooling. Ferrite that has not been changed into austenite would grow up and became coarser when heated. When the heat input was low, the ferrite would grow up slightly. However, the higher heat input would cause the ferrite grains grow larger during welding process. Therefore, the grain size under higher heat input was more non-uniform.

The mixed-grained HAZ of 5100 and 7200 J/cm are characterized by EBSD. We tested the grain size, uniformity, fraction of recrystallization grains of the samples under the highest and lowest heat input, so as to highlight the comparison and emphasize the effect of heat input on microstructural changes. The base metal is also used to compare the change of microstructure after welding. Figure 4a shows the recrystallization maps of base metal. There are a large number of deformed grains after rolling process and the fraction is 39%. During the welding process, part of the deformed grains transformed into austenite and became recrystallized grains after cooling, the dislocation density was lowest. The untransformed deformed grains would undergo recovery process and the dislocation density was also decreased slightly, those deformed grains became substructured grains after welding. Therefore, the number of

deformed grains decreased after welding. When the heat input was 7200 J/cm, the deformed grains have more energy to transform to austenite, and then became recrystallized grains after cooling. Therefore, most of the ferrite were recrystallized grains while substructured grains were few when the heat input was 7200 J/cm. When the heat input was 5100 J/cm, the heat input was so low that only a small part of energy can be provided for the formation of austenite. The residual energy would promote the recovery of deformed grains and become substructured grains after cooling. Hence, the number of substructured grains decrease with the increase in heat input. The deformed grains decrease and the sum of recrystallized and substructured grains in mixed-grained HAZ increase apparently after welding, which confirmed that the dislocation density is greatly reduced. It can also be seen that the substructured grains are larger due to the high temperature under 7200 J/cm. This also verifies the grain nonuniformity under higher heat input.

Effect of heat inputs on the hardness of welded joints

Figure 5a presents the hardness distribution of welded joints in each zone under different heat inputs. The average hardness for each zone of the welded joints is listed in Table 3. It can be seen that the hardness of each region decreases with the increase

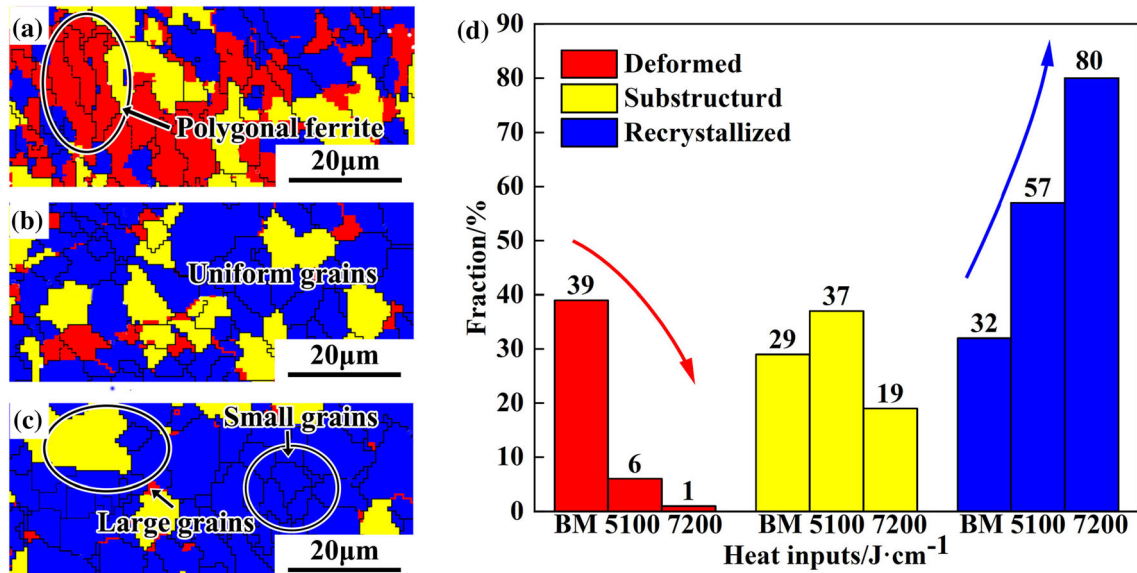


Figure 4 MGHAZ characterization of base metal (BM), 5100 and 7200 J/cm specimens **a–c** EBSD maps of recrystallized, substructured, and deformed grains; **d** fraction of recrystallized, substructured, and deformed grains.

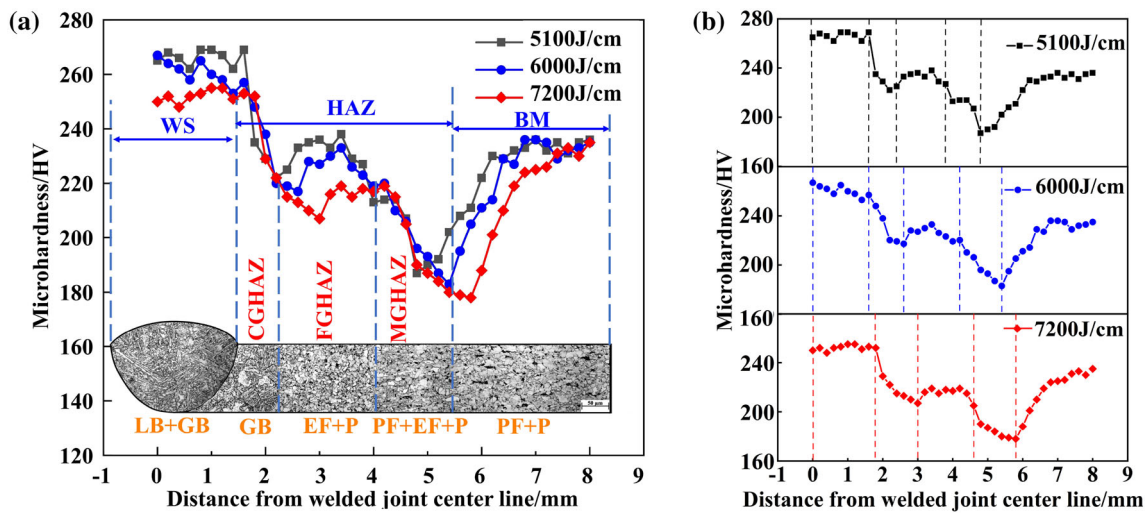


Figure 5 Hardness distribution maps of welded joints under different heat inputs. **a** Hardness distribution maps of three heat inputs; **b** hardness distribution maps of each heat input.

Table 3 Average hardness in each zone of welded joints under different heat inputs

Heat input/J cm ⁻¹	Welded seam	CGHAZ	FGHAZ	MGHAZ	Base metal
5100	266	228	233	207	222
6000	260	228	226	196	224
7200	252	216	215	183	220

in heat input, which is caused by the variation of the microstructure.

The hardness changing trend is the same under three heat inputs (Fig. 5b–d). The highest hardness is in the welded seam, which is due to the high

hardness of lath bainite in this region [32, 33]. In addition, the welding wire has a high content of Mn and Ni. This element would dissolve in the welded seam during the welding process, so the solid solution strengthening in welded seam was increased.

The hardness of coarse-grained HAZ is lower than welded seam owing to the coarsen of microstructure. The microstructure become ferrite in fine-grained HAZ. Generally speaking, the hardness of ferrite is lower than bainite. However, the fine grains formed in this region increase the grain refinement strengthening. Therefore, the hardness of the region not decrease compared with the coarse-grained HAZ. Mixed-grained HAZ is the region with the lowest hardness and also the largest hardness difference exists between this region and base metal. Part of ferrite in this region transformed into austenite and the dislocation was reduced, other untransformed ferrite would grow up and become coarsened. The dislocation and grain refinement strengthening in this region were both reduced, thus to cause the lowest hardness in mixed-grained HAZ. It can also be seen that the hardness in each region decreases with the increase in heat input, which is attributed to the coarsening microstructure.

Effect of heat inputs on strength and plasticity of welded joints

Effect of heat inputs on the strength of welded joints

The engineering stress–strain curve and average mechanical properties of welded joints with different heat inputs are shown in Fig. 6. The yield strength and tensile strength are in the range of 518 to 577 MPa and 630 to 681 MPa, respectively, and the elongation are 10% to 13.6% (Fig. 6b). When the heat

input is 5100 J/cm, the yield strength is 577 MPa and the elongation is 13.6%. The yield strength of base metal is 574 MPa and the elongation is 20.2%. The yield strengths of the 5100 J/cm specimen and base metal are close, but the elongation of 5100 J/cm specimen is lower compared to that of base metal, this is mainly attributed to the non-uniform microstructure in mixed-grained HAZ. When the heat inputs are 6000 and 7200 J/cm, the yield strengths are 541 and 518 MPa, respectively. The yield strengths decrease by 36 and 59 MPa compared with that of the 5100 J/cm specimen, and the elongations also decrease by 1.5% and 3.6%, respectively. It indicates that the mechanical properties of the welded joint decrease with the increase in heat input. As for tensile strength, it is mainly determined by the hard phase in the microstructure. There are more grains with smaller size in the 5100 J/cm sample than that of in the base metal and these grains contributed to the increase in tensile strength. It can also be seen from Fig. 6a that the specimens were fractured at the same position, which is all near the junction of the heat affected zone and the base metal. Combined with the hardness and microstructure analysis, we can conclude that the crack first initiated in mixed-grained HAZ.

The reason for the strength variance under different heat inputs can be explained in combination with microstructure. When the heat input was 5100 J/cm, only part of the microstructure was austenitized and fine grains were obtained after cooling in mixed-grained HAZ. The original polygonal ferrite would

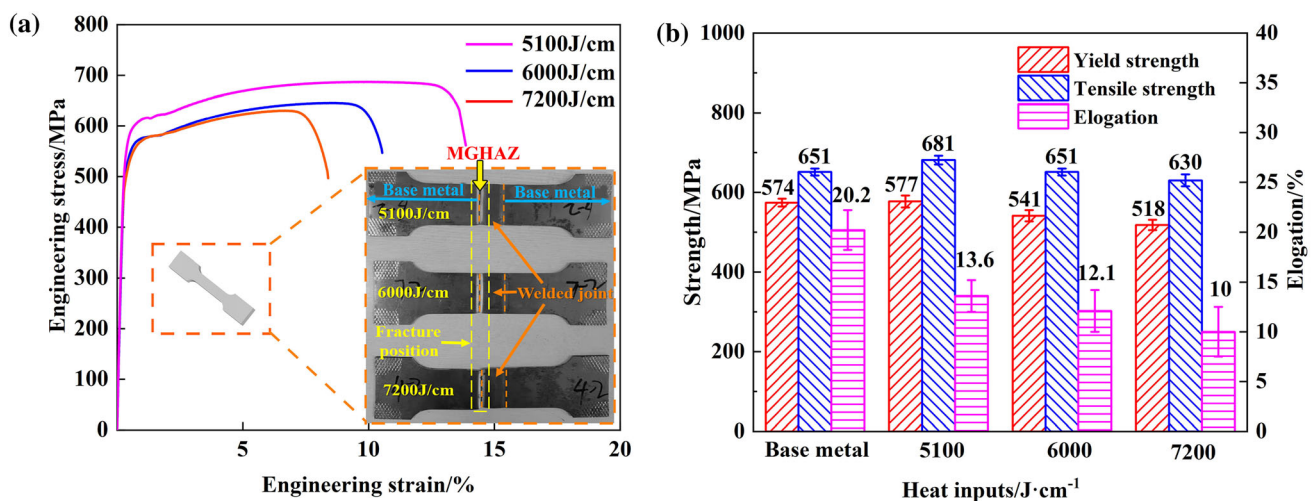


Figure 6 Engineering stress–strain curve and mechanical property of welded joints with different heat inputs. **a** Engineering stress–strain curve; **b** average mechanical property.

become slightly coarser after welding. Therefore, the microstructure of this region consisted of equiaxed ferrite and original fine polygonal ferrite. The grain refinement strengthening compensated the loss caused by the dislocation strengthening, so the yield strength was nearly the same as that of the base metal. However, the sum of recrystallized and substructured grains reached up to 99% when the heat input was 7200 J/cm (Fig. 4c), leading to the great reduction in the dislocation density. Ferrite without austenite transformation would become extremely coarsen at higher temperature, this would lead to the decrease in grain refinement strengthening. As a result, the large grains and small grains with low dislocation density were obtained. The dislocation strengthening and grain refinement strengthening were relatively low when the heat input was 7200 J/cm, causing the decrease in strength. From the perspective of precipitation strengthening, the temperature in this region was so low that the Ti elements cannot be dissolved [20]. Moreover, previous studies showed that the cooling rate after welding was so fast that it would not have a significant effect on the precipitation behavior [34]. It can be inferred that there is little difference between the precipitate behavior under three heat inputs, so the precipitation strengthening is not the reason for strength difference. Based on the above analysis, the reasons caused the strength difference under different heat inputs are attributed to the grain refinement strengthening and dislocation strengthening.

Effect of heat inputs on the plasticity of welded joints

Generally speaking, the increase in strength is accompanied by the decrease in plasticity. However, the strength and plasticity are both the highest when the heat input is 5100 J/cm. The fracture morphology of tensile samples with 5100 and 7200 J/cm heat inputs were observed by SEM and EBSD in order to clarify the reasons for the plasticity difference.

The fracture surfaces with different heat inputs are shown in Fig. 7b, f. All the fracture surfaces of the specimens consist of dimples. It can be seen that they all belong to ductile fracture. It is observed that the 5100 J/cm specimen contains a large fraction of big and deep dimples while the 7200 J/cm specimen has more small and shallow dimples. In the deformation process, the plastic deformation would produce micro cavities. The dimples are formed after these

cavities are nucleated, grown, gathered and finally connected with each other. The formation of large dimple needs more energy and increases the difficulty of fracture, so the plasticity is better when the specimen has more big dimples.

Figure 7c, g shows the microstructure in mixed-grained HAZ of the fractured specimens. It can be seen that the ferrite grains are uniformly elongated and there are few microcracks in the 5100 J/cm specimen, while the ferrite grains are breakage and more microcracks are observed in 7200 J/cm. This is caused by microstructure in mixed-grained HAZ, which can also be verified by the EBSD results shown in Fig. 7h. The grain size near the fracture surface is more non-uniform at 7200 J/cm, resulting in the more uncoordinated deformation during the tensile process. Cracks were more likely to initiate under this heat input, so the plasticity is relatively low. In contrast, the microstructure of base metal is uniform, so the base metal has the highest plasticity. In Fig. 7d, h, the grains oriented in $\langle 111 \rangle // RD$, $\langle 101 \rangle // RD$ and $\langle 001 \rangle // RD$ directions have been simply showed with blue, green and red colors, respectively. It is obvious that the 5100 J/cm specimen has stronger $\langle 111 \rangle // RD$ texture than that of 7200 J/cm specimen. This is because the grains of 5100 J/cm specimen could deformation more coordinately during tensile process, the primary slip enabled the tensile axis to rotate toward the $\langle 111 \rangle$ direction. The $\langle 111 \rangle$ is the close-packed direction of body centered cubic metal, which is beneficial to plastic deformation. Eskandari et al. [35] observed similar texture in high Mn steel, they found that $\langle 111 \rangle$ fibers were strengthened during tensile process. However, there is no obvious texture in 7200 J/cm specimen since the microstructure is quite non-uniform and also the specimen fractured at the earlier stage of tensile process.

Figure 8 shows the schematic of the microstructure for different heat inputs and the crack propagation. The ferrite grains consist of two parts, one is the coarsened and polygonal ferrite transformed from original ferrite (represented in yellow), another is fine and equiaxed ferrite transformed from austenite (represented in gray). When the heat input was low, the original ferrite grew up slightly, so the microstructure in this heat input was relatively uniform. However, the original ferrite would coarsen further under high heat input. Therefore, the microstructure was non-uniform under high heat

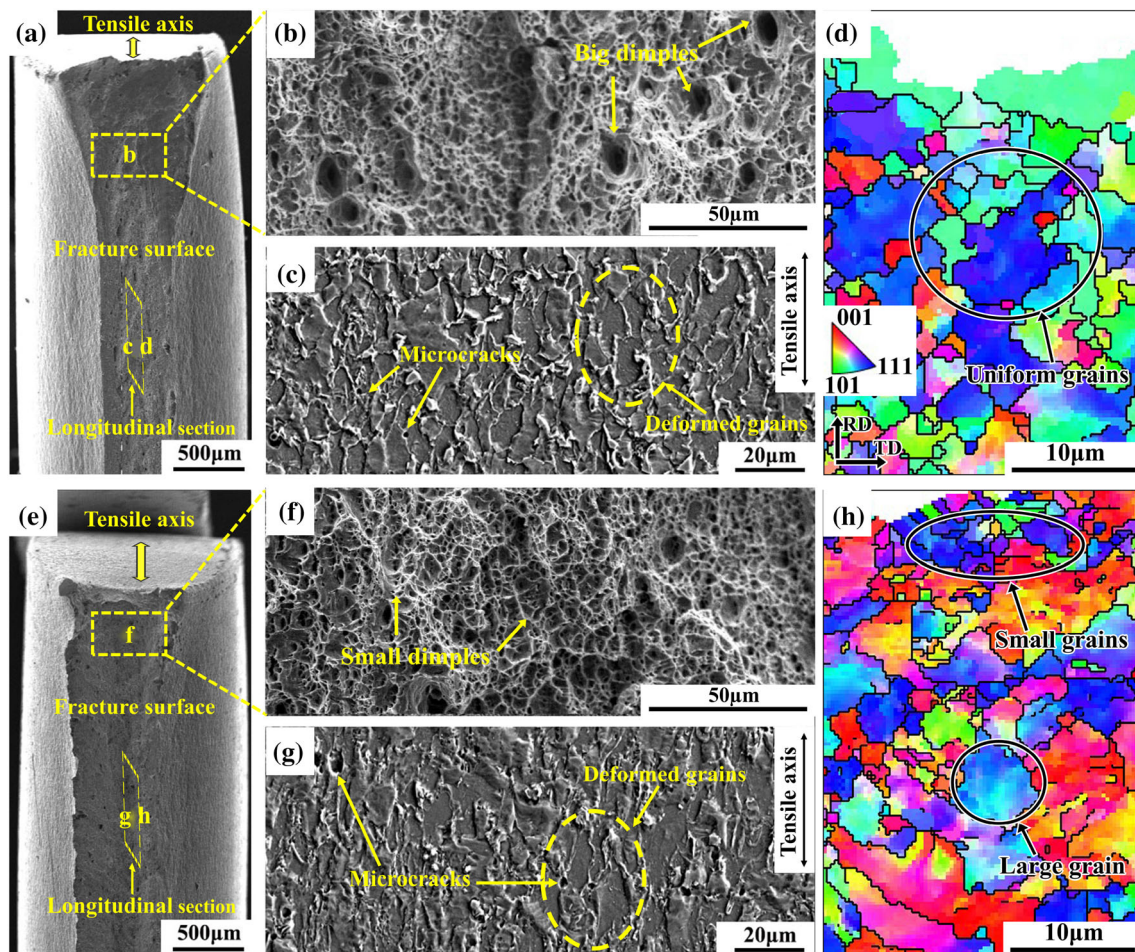


Figure 7 SEM and EBSD images of 5100 and 7200 J/cm specimens. **a, e** The intersection the longitudinal section with the fracture and specimen surface; **b, f** the fracture surface; **c, d, g, h** the longitudinal section.

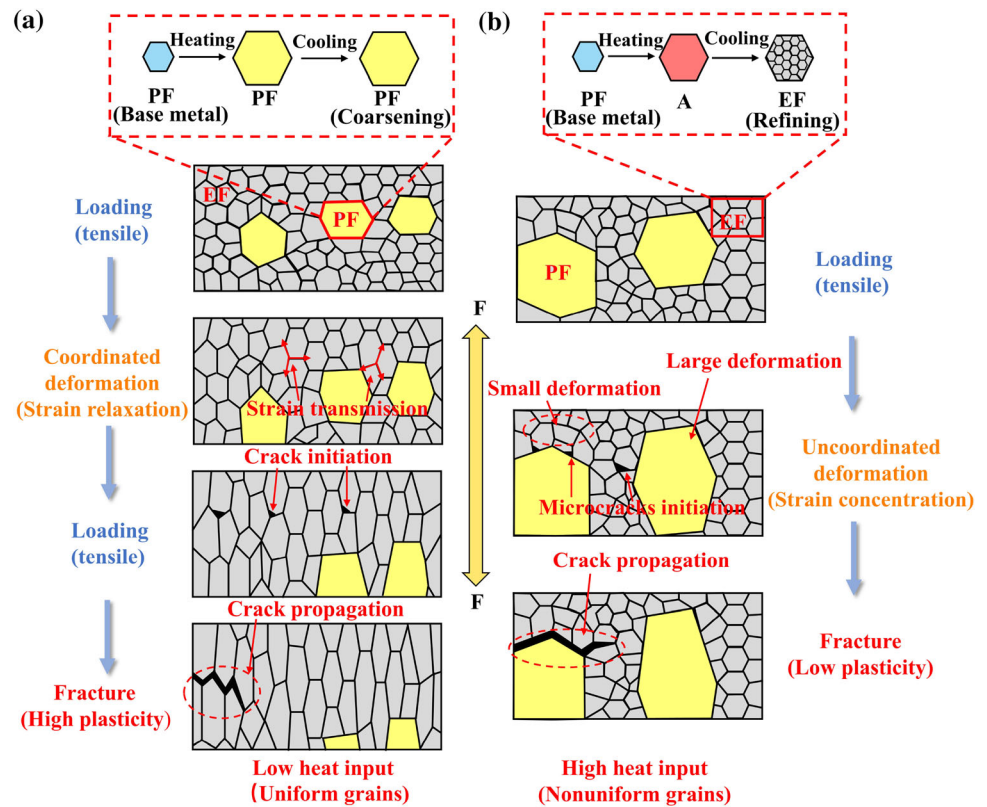
input. The specimen showed better plastic deformation in tensile process due to smaller and more uniform ferrite grains when the heat input was low. This microstructure can promote the strain transmission in the constituent grains, so the coordinated deformation ability during the tensile process was improved [36, 37]. Therefore, the stress concentration was reduced and the plasticity was increased. In contrast, the higher heat input specimen had more non-uniform grains. In the tensile process, the polygonal ferrite had undergone large deformation and the grain was obviously elongated (seen in Fig. 8b), while the equiaxed ferrite had undergone small deformation and the grain had no obvious change. Consequently, the strain was more likely to concentrate in non-uniform ferrite grains due to the absence of an effective coordinated deformation. Therefore, cracks appeared earlier in specimens with high heat input and the plasticity was also decreased.

Conclusion

In this study, the effects of heat input (5100, 6000 and 7200 J/cm) on the microstructure, hardness, strength and plasticity of welded joints are studied. The conclusions are as follows:

1. The microstructure of base metal consisted of polygonal ferrite and small amount of degenerate pearlite. The microstructure of welded seam was lath bainite and granular bainite after welding. The microstructure of CGHAZ and FGHAZ consisted of granular bainite and equiaxed ferrite, respectively. The microstructure of MGHZAZ mainly consisted of two parts: one was and equiaxed ferrite transformed from austenite, the other was coarsened and polygonal ferrite transformed from original ferrite.

Figure 8 Schematic diagram of fracture mechanism under different heat inputs.



- The hardness test result showed that the maximum hardness difference existed between MGHZ and base metal. Parts of the microstructure in MGHZ had undergone austenitizing process and the dislocation strengthening was weakened, the original ferrite became larger and the grain refinement strengthening was also reduced. Therefore, it caused the lowest hardness in MGHZ.
- As the heat input increased from 5100 to 7200 J/cm, the strength decreased by 59 MPa. The amount of austenitized ferrite increased and the original ferrite became coarser with the increase in heat input. Therefore, grain refinement strengthening and dislocation strengthening were both weakened, resulting in the decrease in strength.
- The elongation decreased by 3.6% when the heat input increased from 5100 to 7200 J/cm. The microstructure was relatively uniform when the heat input was 5100 J/cm. However, the original ferrite would become coarser further with the increase in heat input, resulting in the non-uniform microstructure at higher heat input. The 5100 J/cm specimen could deform more coordinately

during tensile process, so it had highest plasticity among three heat inputs.

Acknowledgements

The authors appreciate the financial support from Maanshan Iron & Steel Co. Ltd.

Data availability

All data included in this study are available upon request by contact with the corresponding author.

Declaration

Conflict of interest The authors declare that they have no conflict of interest

References

- Morcillo M, Díaz I, Chico B, Cano H, de la Fuente D (2014) Weathering steels: From empirical development to scientific

- design. A review *Corros Sci* 83:6–31. <https://doi.org/10.1016/j.corsci.2014.03.006>
- [2] Gao XL, Zhu MY, Sun C, Fu GQ (2013) Dynamic recrystallization behavior and microstructure evolution of bridge weathering steel in austenite region. *Steel Res Int* 84(4):377–386. <https://doi.org/10.1002/srin.201200221>
- [3] Jiang ML, Yu W (2019) Study on Continuous Cooling Transformation and Microstructure of 500 MPa Grade Steel for Railway Freight Car Body. *Mater Sci Forum* 944:272–277. <https://doi.org/10.4028/www.scientific.net/MSF.944.272>
- [4] Cheng J, Qing JS, Guo YH, Shen HF (2019) High-strength weathering steels obtained using bainite matrix and nanoscale co-precipitation. *Mater Lett* 236:307–311. <https://doi.org/10.1016/j.matlet.2018.10.076>
- [5] Cui JJ, Zhu WT, Chen ZY, Chen LQ (2020) Microstructural characteristics and impact fracture behaviors of a novel high-strength low-carbon bainitic steel with different reheated coarse-grained heat-affected zones. *Metall Mater Trans A* 51(12):1–11. <https://doi.org/10.1007/s11661-020-06017-3>
- [6] Moon J, Lee CN, Jo HH, Kim SD, Hong HU, Chung JH, Lee BH (2022) Microstructure and high-temperature strength in the weld coarse-grained heat-affected zone of fire-resistant steels and the effects of Mo and Nb additions. *Metal Mater Int* 28(4):966–974. <https://doi.org/10.1007/s12540-020-00947-8>
- [7] Zhen S, Duan ZZ, Sun DQ, Li YX, Gao DD, Li HM (2014) Study on microstructures and mechanical properties of laser-arc hybrid welded S355J2W+ N steel. *Opt Laser Technol* 59:11–18. <https://doi.org/10.1016/j.optlaseng.2013.11.021>
- [8] Kawakubo T, Nagira T, Ushioda K, Fujii H (2021) Friction stir welding of high phosphorus weathering steel-weldabilities, microstructural evolution and mechanical properties. *ISIJ Int* 61(7):2150–2158. <https://doi.org/10.2355/isijinternational.ISIJINT-2021-007>
- [9] Kawakubo T, Ushioda K, Fujii H (2022) Grain boundary segregation and toughness of friction-stir-welded high-phosphorus weathering steel. *Mater Sci Eng A* 832:142350. <https://doi.org/10.1016/j.msea.2021.142350>
- [10] Zhao DW, Bezgans Y, Vdonin N, Kvasnin V (2021) Mechanical performance and microstructural characteristic of gas metal arc welded A606 weathering steel joints. *Int J Adv Manuf Technol* 119(3):1921–1932. <https://doi.org/10.1007/s00170-021-08383-7>
- [11] Wang XN, Zhang SH, Zhou J, Zhang M, Chen CJ, Misra RDK (2017) Effect of heat input on microstructure and properties of hybrid fiber laser-arc weld joints of the 800MPa hot-rolled Nb-Ti-Mo microalloyed steels. *Opt Laser Technol* 91:86–96. <https://doi.org/10.1016/j.optlaseng.2016.11.010>
- [12] Wen CF, Wang ZD, Deng XT, Wang GD, Misra RDK (2018) Effect of heat input on the microstructure and mechanical properties of low alloy ultra-high strength structural steel welded joint. *Steel Res Int* 89(6):1700500. <https://doi.org/10.1002/srin.201700500>
- [13] Wang HB, Wang FL, Shi GH, Sun Y, Liu JC, Wang QF, Zhang FC (2019) Effect of welding heat input on microstructure and impact toughness in CGHAZ of X100Q steel. *J Iron Steel Res Int* 26(6):637–646. <https://doi.org/10.1007/s42243-019-00271-5>
- [14] Deepak JR, Raja VKB, Arputhabalan JJ, Kumar GRY, Thomas SK (2019) Experimental investigation of corten A588 filler rod for welding weathering steel. *Mater Today Proc* 16:1233–1238. <https://doi.org/10.1016/j.matpr.2019.05.219>
- [15] Zhang Y, Shi GH, Sun R, Guo K, Zhang CL, Wang QF (2019) Effect of Si content on the microstructures and the impact properties in the coarse-grained heat-affected zone (CGHAZ) of typical weathering steel. *Mater Sci Eng A* 762:138082. <https://doi.org/10.1016/j.msea.2019.138082>
- [16] Lei JW, Wu KM, Li Y, Huo TP, Xie X, Misra RDK (2019) Effects of Zr addition on microstructure and toughness of simulated CGHAZ in high-strength low-alloy steels. *J Iron Steel Res Int* 26(10):1117–1125. <https://doi.org/10.1007/s42243-019-00319-6>
- [17] You Y, Shang CJ, Subramanian S (2014) Effect of Ni addition on toughness and microstructure evolution in coarse grain heat affected zone. *Metal Mater Int* 20(4):659–668. <https://doi.org/10.1007/s12540-014-4011-4>
- [18] Wang J, Lu SP, Dong WC, Li DZ, Rong LJ (2014) Microstructural evolution and mechanical properties of heat affected zones for 9Cr2WVTa steels with different carbon contents. *Mater Des* 64:550–558. <https://doi.org/10.1016/j.matdes.2014.08.018>
- [19] Odebiyi OS, Adedayo SM, Tunji LA, Onuorah MO (2019) A review of weldability of carbon steel in arc-based welding processes. *Cogent Eng* 6(1):1609180. <https://doi.org/10.1080/23311916.2019.1609180>
- [20] Wang SZ, Gao ZJ, Wu GL, Mao XP (2022) Titanium microalloying of steel: a review of its effects on processing, microstructure and mechanical properties. *Int J Miner Metall Mater* 29(4):645–661. <https://doi.org/10.1007/s12613-021-2399-7>
- [21] Park JY, Ahn YS (2015) Effect of Ni and Mn on the mechanical properties of 22Cr micro-duplex stainless steel. *Acta Metall Sin* 28(1):32–38. <https://doi.org/10.1007/s40195-014-0162-z>
- [22] Zhang H, Zhang CH, Wang Q, Wu CL, Zhang S, Chen J, Ao A (2018) Effect of Ni content on stainless steel fabricated by

- laser melting deposition. *Opt Laser Technol* 101:363–371. <https://doi.org/10.1016/j.optlastec.2017.11.032>
- [23] Li DL, Fu GQ, Zhu MY, Li Q, Yin CX (2018) Effect of Ni on the corrosion resistance of bridge steel in a simulated hot and humid coastal-industrial atmosphere. *Int J Miner Metall Mater* 25(3):325–338. <https://doi.org/10.1007/s12613-018-1576-9>
- [24] Lan LY, Qiu CL, Zhao DW, Gao XH, Du LX (2012) Analysis of martensite–austenite constituent and its effect on toughness in submerged arc welded joint of low carbon bainitic steel. *J Mater Sci* 47(11):4732–4742. <https://doi.org/10.1007/s10853-012-6346-x>
- [25] Amer AE, Koo MY, Lee KH, Kim SH, Hong SH (2010) Effect of welding heat input on microstructure and mechanical properties of simulated HAZ in Cu containing microalloyed steel. *J Mater Sci* 45(5):1248–1254. <https://doi.org/10.1007/s10853-009-4074-7>
- [26] Lee WH (2007) Weld metal hydrogen-assisted cracking in thick steel plate weldments. *Mater Sci Eng A* 445:328–335. <https://doi.org/10.1016/j.msea.2006.09.046>
- [27] Venkatesan MV, Murugan N, Sam S, Albert SK (2014) Effect of heat input on macro, micro and tensile properties of flux cored arc welded ferritic stainless steel joints. *Trans Indian Inst Met* 67(3):375–383. <https://doi.org/10.1007/s12666-013-0358-3>
- [28] Siltanen J, Tihinen S, Komi J (2015) Laser and laser gas-metal-arc hybrid welding of 960 MPa direct-quenched structural steel in a butt joint configuration. *J Laser Appl* 27(S2):S29007. <https://doi.org/10.2351/1.4906386>
- [29] Olasolo M, Uranga P, Rodriguez-Ibabe JM, Lopez B (2011) Effect of austenite microstructure and cooling rate on transformation characteristics in a low carbon Nb–V microalloyed steel. *Mater Sci Eng A* 528(6):2559–2569. <https://doi.org/10.1016/j.msea.2010.11.078>
- [30] Lan LY, Qiu CL, Zhao DW, Gao XH, Du LX (2013) Effect of reheat temperature on continuous cooling bainite transformation behavior in low carbon microalloyed steel. *J Mater Sci* 48(12):4356–4364. <https://doi.org/10.1007/s10853-013-7251-7>
- [31] Sun Q, Di HS, Li JC, Wu BQ, Misra RDK (2016) A comparative study of the microstructure and properties of 800 MPa microalloyed C-Mn steel welded joints by laser and gas metal arc welding. *Mater Sci Eng A* 669:150–158. <https://doi.org/10.1016/j.msea.2016.05.079>
- [32] Zhou Y, Chen SY, Chen XT, Cui T, Liang J, Liu CS (2019) The evolution of bainite and mechanical properties of direct laser deposition 12CrNi2 alloy steel at different laser power. *Mater Sci Eng A* 742:150–161. <https://doi.org/10.1016/j.msea.2018.10.092>
- [33] Tang G, Zhao X, Li RD, Liang Y, Jiang YS, Chen H (2019) Microstructure and properties of laser-arc hybrid welding thick bainitic steel joints with different arc position. *Mater Res Express* 6(7):076547. <https://doi.org/10.1088/2053-1591/ab1557>
- [34] Wang HH, Qin ZP, Wan XL, Wei R, Wu KM, Misra D (2017) Continuous cooling transformation behavior and impact toughness in heat-affected zone of Nb-containing fire-resistant steel. *Metal Mater Int* 23(5):848–854. <https://doi.org/10.1007/s12540-017-6776-8>
- [35] Eskandari M, Mohtadi-Bonab MA, Zarei-Hanzaki A, Szpunar JA, Basu R (2019) Texture and microstructure development of tensile deformed high-Mn steel during early stage of recrystallization. *Phys Metal Metallogr* 120(1):32–40. <https://doi.org/10.1134/S0031918X19010034>
- [36] Gao ZJ, Li JY, Feng ZH, Wang YD (2019) Influence of hot rolling on the microstructure of lean duplex stainless steel 2101. *Int J Miner Metall Mater* 26(10):1266–1273. <https://doi.org/10.1007/s12613-019-1841-6>
- [37] Zhou LY, Jiang B, Cui TH, Zhang D, He JZ, Liu YZ (2014) Effect of strengthening phase on deformation behavior during uniaxial tension of hot-rolled dual phase steel. *J Iron Steel Res Int* 21(12):1111–1115. [https://doi.org/10.1016/S1006-706X\(14\)60191-6](https://doi.org/10.1016/S1006-706X(14)60191-6)

Publisher's Note Springer Nature remains neutral with regard to jurisdictional claims in published maps and institutional affiliations.

Springer Nature or its licensor holds exclusive rights to this article under a publishing agreement with the author(s) or other rightsholder(s); author self-archiving of the accepted manuscript version of this article is solely governed by the terms of such publishing agreement and applicable law.